IET Radar, Sonar & Navigation

Research Article

Contribution of auxiliary coherent radar receiver to target's velocity estimation

ISSN 1751-8784
Received on 2nd July 2017
Revised 2nd November 2017
Accepted on 4th November 2017
E-First on 7th December 2017
doi: 10.1049/iet-rsn.2017.0299
www.ietdl.org

Itzik Cohen[1], Nadav Levanon[1] ✉

[1]*Electrical Engineering – Systems, Tel-Aviv University, Tel-Aviv, Israel*

✉ *E-mail: nadav@eng.tau.ac.il*

Abstract: Recent progress in bistatic radar techniques can be used to improve performances of classical monostatic radar. A prominent limitation of coherent radar is its inability to measure the complete velocity vector (magnitude and direction) of a detected target. A single coherent detection can provide range-rate only. At least two detections, separated in time, are needed to estimate the target's velocity vector. This study discusses how the velocity vector can be determined by two simultaneous detections spaced in distance. The second detection is obtained by an auxiliary distant bistatic coherent receiver; an approach proposed in the 1990s to enhance meteorological radar. Being a very simple case of a distributed radar system allows for a simple demonstration of how to calculate the target's position and velocity vector and how to analyse the estimation accuracy, including geometric dilution of precision plots of the velocity error. Also discussed are two methods to identify correct data association when more than one target is detected.

1 Introduction

Single detection of a target by basic monostatic two-dimensional (2D) coherent radar can estimate the target's azimuth, range and range rate. Position resolution depends on the waveform's bandwidth and the antenna beamwidth. Range-rate resolution depends on the duration of the coherent processing interval. A single measurement of position and range rate does not provide complete target motion information (velocity magnitude and velocity direction). As Fig. 1 shows, a specific range rate can fit infinitely many velocity vectors (red lines). This paper demonstrates how data from simultaneous detection by an auxiliary, coherent, bistatic receiver, can select the true velocity vector (black arrow).

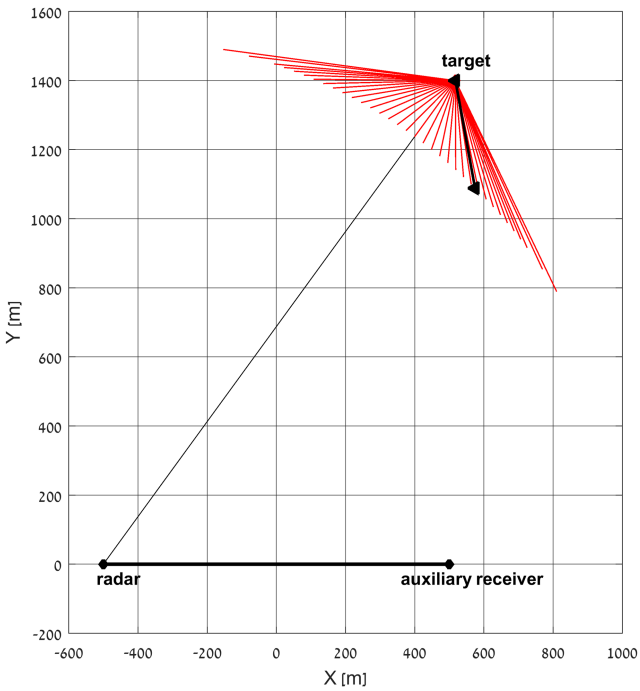

Fig. 1 *Contribution of the auxiliary receiver*

Fig. 2 shows that an iso-range-rate contour (a solid black line) is simply a straight line on the v_x, v_y plane, perpendicular to the radial direction to the radar (dashed red line), determined by the antenna pointing direction. Fig. 2 also shows (diamond markers) several velocity vectors, all corresponding to the same range rate of −10 m/s.

If velocity magnitude and direction are needed from monostatic radar, at least two repeated measurements are required, spaced in time (tracking). Our paper considers an alternative approach – the two measurements are spaced geographically. The second measurement is taken simultaneously by an auxiliary bistatic coherent receiver. The receiver receives both the direct radar transmission and the delayed reflection from the target. Fig. 3 describes the scene this paper considers. Using a remote bistatic receiver to retrieve vector winds was proposed and tested together with meteorological radar [1–3]. In meteorological applications, the target is relatively large atmospheric volume containing precipitation particles. Separate passive radar receivers have been used for many other applications, most prominently in air defence [4], where other issues like extending range and covert operation were the motivation. To continuously support primary radar when its antenna beam changes direction, the antenna of the auxiliary receiver needs to have wide beamwidth. A wide-beamwidth low-gain antenna is simple to implement but implies short-range applications. Long-range applications of separate bistatic receiver (not considered here), which requires high-gain narrow-beam antenna, can utilise the complex technique of 'pulse chasing' [4, Section 13.2].

Recent technical progress in bistatic radar [5, 6] prompts adapting the idea used in meteorology to point-like moving targets, several of which can exist within the volume considered in meteorology. The system considered here is perhaps the simplest case of a 2D distributed radar system (DRS). To keep the radar system simple, the auxiliary receiver makes its own coherent detections on a (bistatic) range/range-rate map, namely on a $r_b, \dot{r}_b$ plane, where r_b is defined in (1) or (3). It then relays those two measurements, for each detected target, to the primary radar processor. This concept is termed decentralised radar network (DRN) [5], or non-coherent DRS [7, 8]. When the distance to the auxiliary receiver is relatively small, different approaches for transferring auxiliary receiver data to the main radar can be used, like optical fibre [9] or microwave link [10].

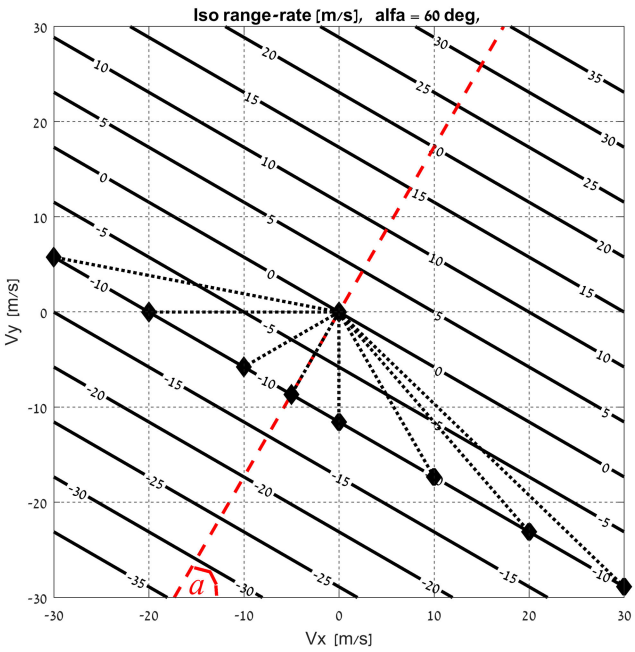

Fig. 2 *Iso-range-rate contours on the v_x, v_y plane and several velocity vectors with $\dot{r} = -10$ m/s*

The scene in Fig. 3 contains: the radar transmitter and receiver (point A), the auxiliary receiver (point B), the baseline (b), two iso-range contours (solid, black, circles) from the radar (r_1) and two contours (dash, red, ellipses) of half the iso-bistatic-range

$$(r_1 + r_2 - b)/2 = (r_b - b)/2 \tag{1}$$

The shaded area around the target area (point C) represents a position resolution cell defined by the four contours. That cell will be referred to as a 'bistatic azimuth resolution'. This resolution is geometry dependent. In most cases, the radar's 'intrinsic antenna azimuth resolution' will be much better than the 'bistatic azimuth resolution'. The latter will not help in estimating the target's position, but will play an important role in measurements association.

The more important contribution of the auxiliary receiver is expanding the scalar range rate $\dot{r}_1$ into a vector $[v_x, v_y]$ describing the target velocity along the two axis X and Y. That additional information requires that in addition to the range-rate measurement $\dot{r}_1$, performed by the radar receiver, the auxiliary receiver will measure the bistatic range rate $\dot{r}_b$. The four target's unknowns $\boldsymbol{x} = [x, y, v_x, v_y]^{\mathrm{T}}$, can be solved by least squares, using the five measurements $z = [r_1, r_b, \dot{r}_1, \dot{r}_b, \alpha]^{\mathrm{T}}$, where α is the radar's antenna beam direction. Direct expressions of $\boldsymbol{x}$ can be derived when only four measurements are used, e.g. $[r_1, \dot{r}_1, \dot{r}_b, \alpha]$.

The simplicity of the system: one coherent 2D radar with narrow-beam antenna and one remote coherent receiver with wide-beam antenna makes it relatively practical to implement and simple to analyse, including in case of more than one target, which more general discussions [e.g. 7, 8] avoid.

The following sections will: (i) describe how to solve $\boldsymbol{x}$ given z; (ii) present Monte-Carlo simulation results of the expected error spread of the elements of $\boldsymbol{x}$; (iii) display a contour plot of the geometric dilution of precision (GDOP) of the calculated velocity; (iv) suggest incoherent fusion of targets' data, when several targets are detected simultaneously.

It is difficult to predict future use of an idea, but we feel that the advantage of the proposed concept is in short-range radar applications, where the radar scene changes rapidly and does not allow calculating the target velocity vector over multiple dwells.

2 Solving target's parameters

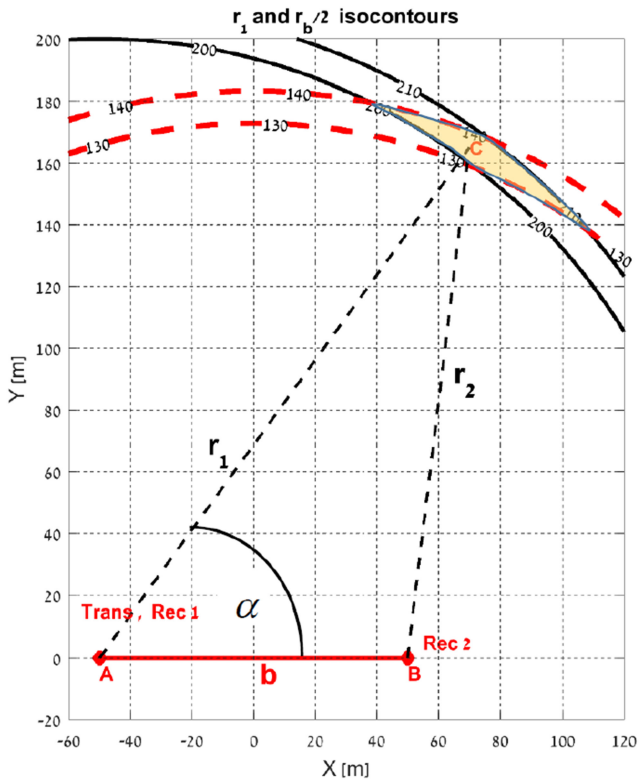

Fig. 3 *Bistatic radar scene*

Direct analytical non-linear expressions for $z = \boldsymbol{h}(\boldsymbol{x})$ can be easily derived and are given below. Due to the non-linearity the inverse operation can preferably be solved iteratively using a simple least-squares algorithm (Gauss–Newton method) [11], which will be outlined also.

Let the radar coordinates be given by (x_1, y_1), the auxiliary receiver by (x_2, y_2), the target by (x, y) and the baseline length by b. The resulted ranges are given by

$$r_i = \left[(x - x_i)^2 + (y - y_i)^2\right]^{1/2}, \quad i = 1, 2 \tag{2}$$

$$r_b = r_1 + r_2 \tag{3}$$

The range rates $\dot{r}_1$ and $\dot{r}_b$ are measured through the Doppler shifts of the returns at each of the receivers, and the angle to the target α is the angle measured from the radar's transmitter/receiver. The measurements are hampered by errors, represented by the five-element vector $\boldsymbol{u}$, thus

$$z = \boldsymbol{h}(\boldsymbol{x}) + \boldsymbol{u} \tag{4}$$

Following Gauss' method of linearisation, we use the 5×4 partial derivative matrix $\boldsymbol{H}$ (see Appendix)

$$\boldsymbol{H} = \boldsymbol{H}(\boldsymbol{x}) = \frac{\partial \boldsymbol{h}}{\partial \boldsymbol{x}}(\boldsymbol{x}) \tag{5}$$

and apply the iterative algorithm

$$\hat{\boldsymbol{x}}_{k+1} = \hat{\boldsymbol{x}}_k + \left(\hat{\boldsymbol{H}}^{\mathrm{T}} \boldsymbol{W} \hat{\boldsymbol{H}}\right)^{-1} \hat{\boldsymbol{H}}^{\mathrm{T}} \boldsymbol{W}(z - \hat{z}) \tag{6}$$

Normally, $\boldsymbol{W}$ is obtained from the inverse of the covariance of the measurements error vector

$$\boldsymbol{W} = \Lambda^{-1} = \left(\mathrm{cov}\{\boldsymbol{u} \cdot \boldsymbol{u}^{\mathrm{T}}\}\right)^{-1} \tag{7}$$

If the different elements of the noise vector $\boldsymbol{u}$ are independent, $\boldsymbol{W}$ simplifies to a diagonal matrix

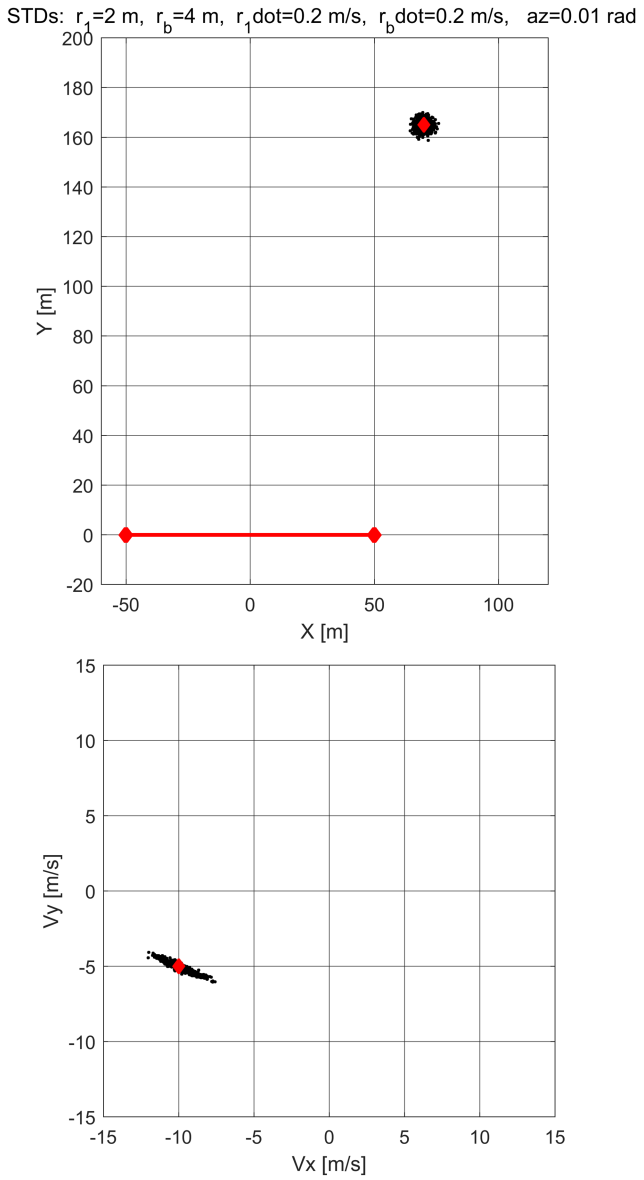

Fig. 4 *Simulation results with azimuth measurement: (top) position, (bottom) velocity*

$$\text{diag } \boldsymbol{W} = \left\{\sigma_{r_1}^{-2} \quad \sigma_{r_b}^{-2} \quad \sigma_{\dot{r}_1}^{-2} \quad \sigma_{\dot{r}_b}^{-2} \quad \sigma_{\alpha}^{-2}\right\} \tag{8}$$

where σ_l^2 is the standard deviation of the noise element of the measurement l (where l is $r_1, r_b, \dot{r}_1, \dot{r}_b$ and α).

$\boldsymbol{W}$ can provide means to emphasise the influence of specific measurements upon $\hat{\boldsymbol{x}}$, the estimated unknowns. For example, if the radar antenna beamwidth is relatively wide, $\boldsymbol{W}_{5,5}$ will be assigned a small value, while if the beamwidth is narrow $\boldsymbol{W}_{5,5}$ will be increased, while $\boldsymbol{W}_{2,2}$ (the weight of the bistatic range r_b) can be decreased.

$\hat{\boldsymbol{x}}_k$ and $\hat{\boldsymbol{x}}_{k+1}$ are the current and next target's position and velocity estimates. The subscript k represents the iteration number, with $k = 0$ representing the first guess

$$\hat{\boldsymbol{H}} = \boldsymbol{H}(\hat{\boldsymbol{x}}_k) \tag{9}$$

is the partial derivative matrix calculated at the current target's position and velocity estimates, and

$$\hat{z} = \boldsymbol{h}(\hat{\boldsymbol{x}}_k) \tag{10}$$

are the expected error-free measurements calculated using the current target's position and velocity estimates. Normally, the iterations terminate when the correction from $\hat{\boldsymbol{x}}_k$ to $\hat{\boldsymbol{x}}_{k+1}$ becomes negligible. Our simulations show that, for a reasonable first guess, 10–20 iterations will suffice.

From the discussion above we might incorrectly conclude that having a rotating narrow-beam radar antenna diminishes the value of the bistatic range measurement r_b. Such a conclusion will not hold in a practical scenario, where there are likely to be several moving targets. Prior to processing the detection information from the two sources (radar and auxiliary receiver), the processor needs to perform registration of targets. Namely, pair the same target data from the two sources. Such pairing will rely heavily on the r_b measurement, obtained by the auxiliary receiver.

3 Simulation results

The spread of estimated target positions (x, y) and velocities (v_x, v_y) was obtained from Monte-Carlo simulations. Each simulation was repeated 500 times with different random measurement errors taken from $N(0, \sigma_i^2)$, $i = 1, 2, \ldots, 5$. The standard deviations σ_i of the measurements errors are listed in the figures' titles. Fig. 4 was obtained using all five measurements (azimuth included). The diagonal elements of the weight matrix $\boldsymbol{W}$ were set to

$$\text{diag } \boldsymbol{W} = \{1 \quad 0.001 \quad 1 \quad 1 \quad 1000\} \tag{11}$$

Note the small value of $\boldsymbol{W}_{2,2}$ (the weight assigned to the bistatic range r_b) and the large value of $\boldsymbol{W}_{5,5}$ (the weight assigned to the angle α). The small weight assigned to the bistatic range measurement r_b does not imply that this measurement is not needed. It is crucial to the proper registration of detected targets in both sites. The true target parameters: $x = 70\,\text{m}, y = 165\,\text{m}, v_x = -10\,\text{m/s}, v_y = -5\,\text{m/s}$, appear as red markers on the drawings. Fig. 4 demonstrates the performances when the radar utilises narrow antenna beamwidth. The beamwidth influences not only the accuracy of the estimated position but also the accuracy of the estimated target velocity vector, although without the auxiliary receiver a velocity vector (v_x, v_y) will not be available at all, only the range rate $\dot{r}_1$ would.

4 GDOP plots

The Monte-Carlo simulations described in the previous section applied to one location. A more general picture of the expected performances (position and velocity resolutions and accuracies) over a larger geometrical map can be obtained by using contour maps of the GDOP [12–14]. In our five measurement case, two measurements are in distance units (m), two in velocity units (m/s) and the fifth is in radians. For such a case, the position GDOP (GDOP-P) and the velocity GDOP (GDOP-V) can be defined as

$$\text{GDOP} - \text{P} = \sqrt{\boldsymbol{G}_{1,1} + \boldsymbol{G}_{2,2}} \tag{12}$$

$$\text{GDOP} - \text{V} = \sqrt{\boldsymbol{G}_{3,3} + \boldsymbol{G}_{4,4}} \tag{13}$$

where

$$\boldsymbol{G} = \left(\boldsymbol{H}^{\text{T}}\, \boldsymbol{W}\, \boldsymbol{H}\right)^{-1} \tag{14}$$

The diagonal weight matrix $\boldsymbol{W}$ reflects the different measurement errors and the importance assigned to a specific measurement. Thus, to describe the estimation without using the radar antenna beamwidth we would have selected $\text{diag}(\boldsymbol{W}) = [1 \quad 1 \quad 1 \quad 1 \quad 1/1000]$, while when using an azimuth measurement we selected $\text{diag}(\boldsymbol{W}) = [1 \quad 0.0001 \quad 1 \quad 1 \quad 10000]$. When using the latter $\boldsymbol{W}$ the resulted GDOP-V is as presented in Fig. 5. The GDOP-V plot shows relatively small GDOP-V in a direction perpendicular to the baseline, increasing towards the directions of the baseline. Fig. 5 matches Fig. 4*b* in [3].

5 Fusion

We assume that both the radar and the auxiliary receiver include moving target indicators (MTI) and good pulse-Doppler

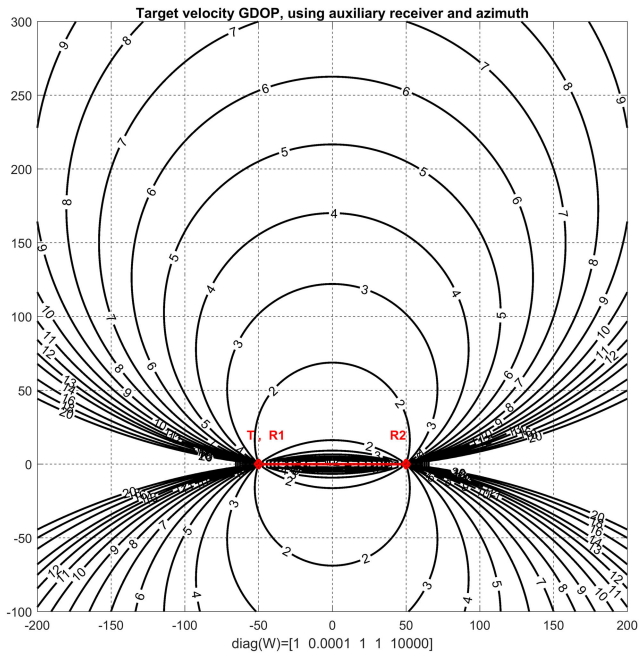

Fig. 5 *GDOP-V contours when using azimuth measurement. Cartesian coordinates in meters*

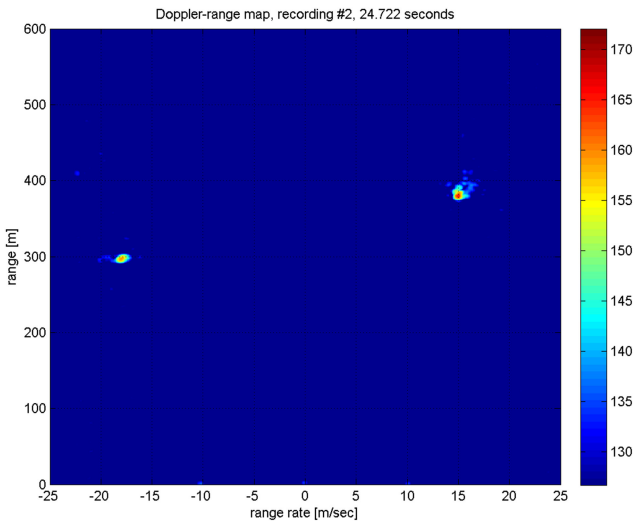

Fig. 6 *Bistatic receiver output on a range/range-rate display with two moving targets (colour bar in dB)*

processing, hence eliminate stationary clutter. Even when the radar uses a narrow-beam antenna, it is likely that more than one moving target will be simultaneously illuminated and detected by the radar and the auxiliary receiver. Since the gain of the wide-beamwidth auxiliary receiver's antenna is expected to be relatively small, it is possible that not all the targets detected by the radar receiver will be detected by the auxiliary receiver.

Fig. 6 displays a range/range-rate output (in dB) obtained experimentally [15] by a bistatic coherent receiver. The scene contained two moving targets (cars), one approaching and one receding. The Doppler processor contained MTI circuitry that removed the strong clutter column around zero range rate. CFAR detection will produce range and range-rate numbers for each one of the two targets. In Fig. 6 range is $(r_b - b)/2$.

To be able to use both detections and get the benefits described in the previous sections, the central processing has to pair simultaneous detections, obtained at the two receivers, to belong to the same target. Such fusion is far from being trivial.

One option is to pair each detection and related measurements by one receiver with all the detections by the other receiver, and pick the correct pair. We will consider that approach assuming two targets detected in both receivers. The radar scene used to

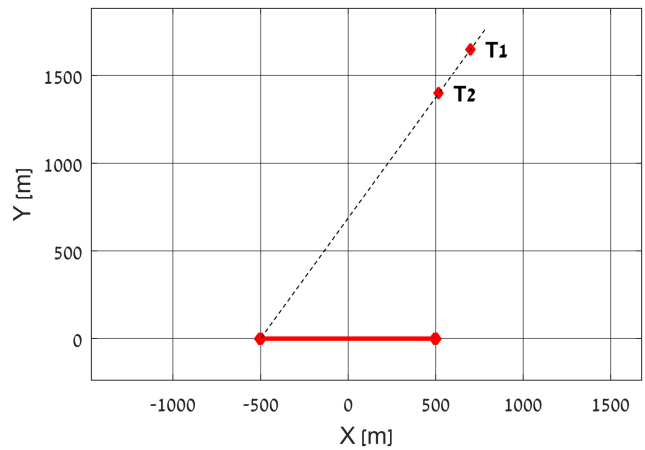

Fig. 7 *Radar scene with two targets*

Table 1 Targets associated with measurement sources

Case	1	2	3	4
Source and measurements	Fig. 8		Figs. 9, 10	
radar: $r_1, \dot{r}_1, \alpha$	T_1	T_2	T_1	T_2
auxiliary receiver: r_b, $\dot{r}_b$	T_1	T_2	T_2	T_1

demonstrate fusion is depicted in Fig. 7. It is on a larger geometric scale than used in the previous section. The base line is 1000 m long. The two targets T_1 and T_2 are placed on the same azimuth line from the radar, as expected if both are simultaneously illuminated by a narrow beam radar antenna.

Four cases were simulated and are listed in Table 1. Case #1 is shown in Fig. 8. The measurements from target 1 (T_1), in both receivers, were associated correctly. The top subplot shows the resulted target position estimates after 500 Monte-Carlo simulation runs. The bottom subplot shows the velocity vector estimation results. Note the estimation results (black dots) surrounding the true values (red diamonds). Note (top subplot) that the estimated positions are spread around the true target position, while the estimated velocity values (bottom subplot) are spread along a line with the true velocity value at its centre. In case #2, the measurements from target 2 were associated correctly. The results (not shown) exhibit the same behaviour as in Fig. 8, but around T_2 and V_2. Results from an erroneous association (case #3) are presented in Figs. 9 and 10, which differ by the $\boldsymbol{W}$ used. In case #3, the measurements by the radar are related to target 1 and the measurement by the auxiliary receiver are related to target 2. We see that the position determination remains almost correct, near $T1$, because it is mostly determined by the radar measurements r_1, α, while the velocity vector determination is shifted towards V_2, because $r_b, \dot{r}_b$ were taken from target T_2. A similar outcome (not shown) was observed for case #4.

Note that in the estimation algorithm in this section we used $\text{diag}(\boldsymbol{W}_a) = [1 \quad 0.0001 \quad 1 \quad 1 \quad 10,000]$, while the measurements vector was $\boldsymbol{z} = [r_1, r_b, \dot{r}_1, \dot{r}_b, \alpha]^{\mathrm{T}}$. The very small weight assigned to the bistatic range r_b is responsible for the fact that in Figs. 8 and 9 the measured positions of T_1 are almost the same, despite the fact that in Fig. 9 r_b applies to the wrong target T_2. If we repeat the estimation using a weight matrix $\boldsymbol{W}_{\mathrm{b}}$ giving more weight to r_b and less to α, such as $\text{diag}(\boldsymbol{W}_b) = [1 \quad 1 \quad 1 \quad 1 \quad 0.001]$, the resulted estimation for case #3 becomes dramatically different (Fig. 10).

The estimated position in Fig. 10 is ~1200 m off the true position. If that modified weight matrix would have been applied to case #1 (correct assignment) the change in the estimated T_1 position would have been smaller than 20 m.

The above results suggest a possible indication of an erroneous association: perform two target position estimations using the two different weight matrices $\boldsymbol{W}_a$ and $\boldsymbol{W}_b$. If the two resulted target positions are very close to each other the measurement association

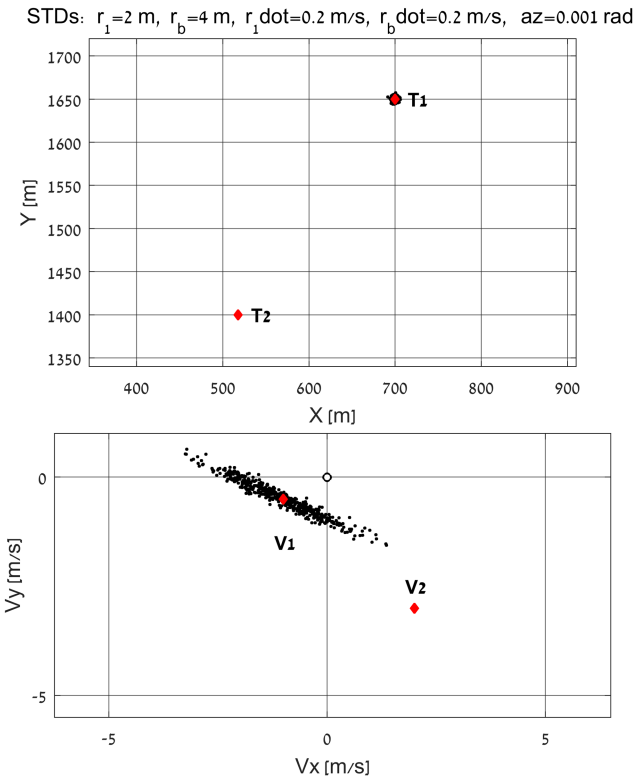

Fig. 8 *Two target scene, correct fusion related to target 1 (case#1)*

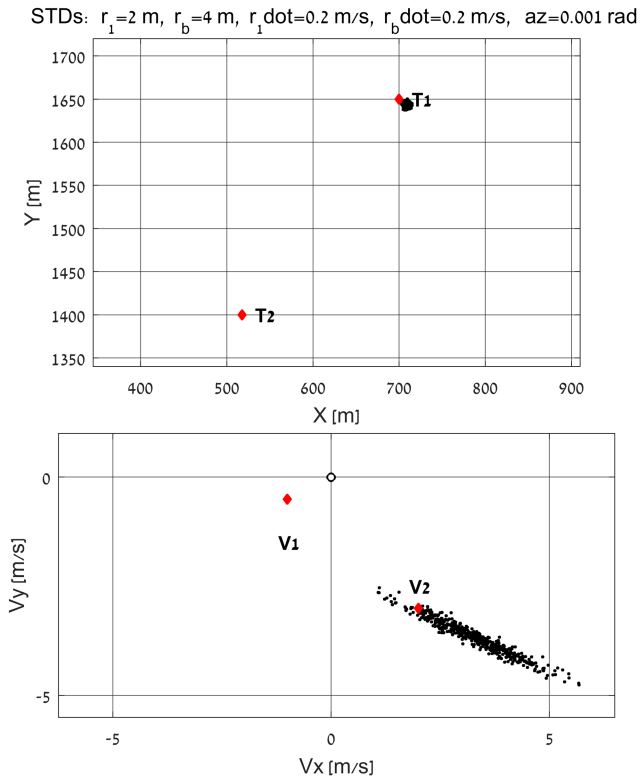

Fig. 9 *Two target scene, erroneous fusion (case#3)* $\mathrm{diag}(\boldsymbol{W}_a) = [1 \quad 0.0001 \quad 1 \quad 1 \quad 10000]$

is correct. Then accept the position and velocity results obtained with $\boldsymbol{W}_a$.

An alternative approach to identify erroneous association is to run the estimation algorithm using a weight matrix $\boldsymbol{W}_c$ that is the inverse of the expected measurements error covariance matrix, defined in (7), and then calculate the normalised residual (the fit error)

$$\varepsilon^2 = (z - \hat{z})^{\mathrm{T}} \boldsymbol{W}_{\mathrm{c}} (z - \hat{z}) \tag{15}$$

where $\hat{z}$ are the measurements expected from the last position and velocity estimates $\hat{\boldsymbol{x}}$. Small residual implies correct association.

Fig. 11 shows the probability density functions (PDFs) of the residuals obtained from 500 Monte-Carlo trials. The top subplot applies to case #1 (correct association). The bottom subplot applies to case #3 (erroneous association). The very large separation between the two PDFs indicates that it will be relatively simple to set a threshold that will guarantee correct decision after a single detection. The weight matrix used to obtain Fig. 11 was $\mathrm{diag}(\boldsymbol{W}_c) = \left[1\mathrm{m}^{-2} \quad 1\mathrm{m}^{-2} \quad 1(\mathrm{m/s})^{-2} \quad 1(\mathrm{m/s})^{-2} \quad (\pi/180)^{-2}\mathrm{rad}^{-2}\right]$.

After correct fusion the available output contains the positions of the two targets and their respective velocity vectors. An example appears in Fig. 12. To make the velocity vector more readable it appears as a line extending from the estimated target position to where the target will be after Δt seconds ($\Delta t = 40$ s was used in Fig. 12) and assuming no manoeuvring. Fig. 12 contains the outcome of seven simulation runs.

6 Conclusions

In order to determine the velocity magnitude and direction of a target, conventional 2D coherent radar needs at least two measurements spaced in time. Our paper shows how velocity can be determined by two simultaneous measurements spaced in distance. The target's velocity magnitude and direction, rather than just its range rate, can be obtained by additional simultaneous measurements from an auxiliary bistatic coherent receiver. The auxiliary receiver needs to receive both the radar signal, through direct reception (or physical link) and the signal reflected from the target; coherently detect the target and relay its estimate of the bistatic range and range rate, to the radar's processor. Fig. 6, taken

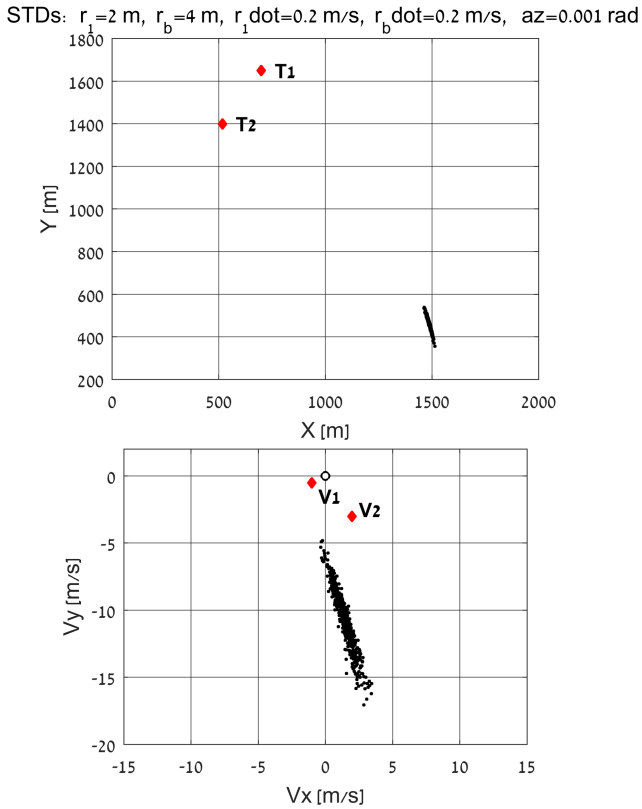

Fig. 10 *Two target scene, erroneous fusion (case#3)* $\mathrm{diag}(\boldsymbol{W}_a) = [1 \quad 1 \quad 1 \quad 1 \quad 0.001]$

from experiments described in [15], presented an example of such measurements.

Coherent detection at the auxiliary receiver involves oscillators' synchronisation, which is a major topic by itself that we did not expand on. We only point out that some systems use global positioning system [16] and some use direct detection [17].

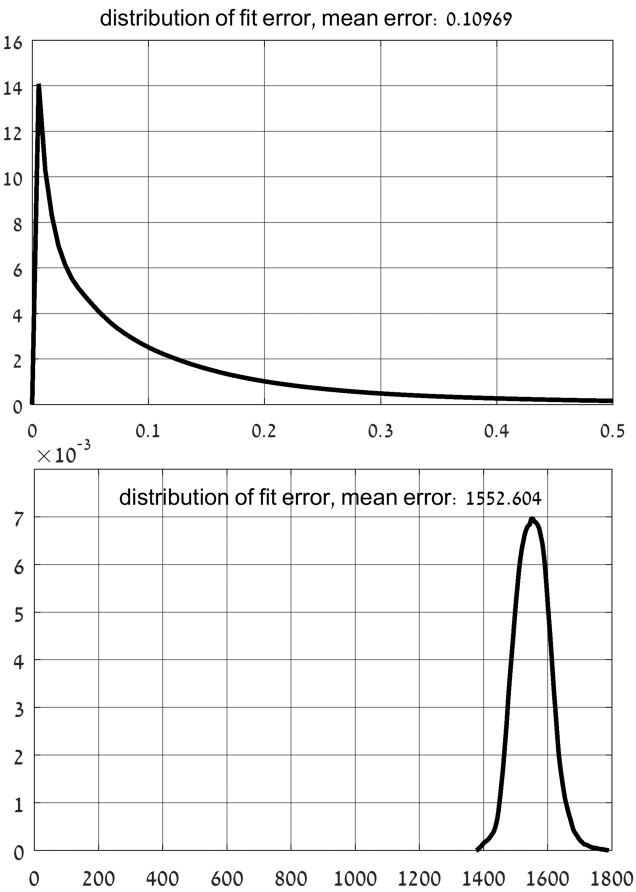

Fig. 11 *PDF of fit error, (top) case #1, (bottom) case #3*

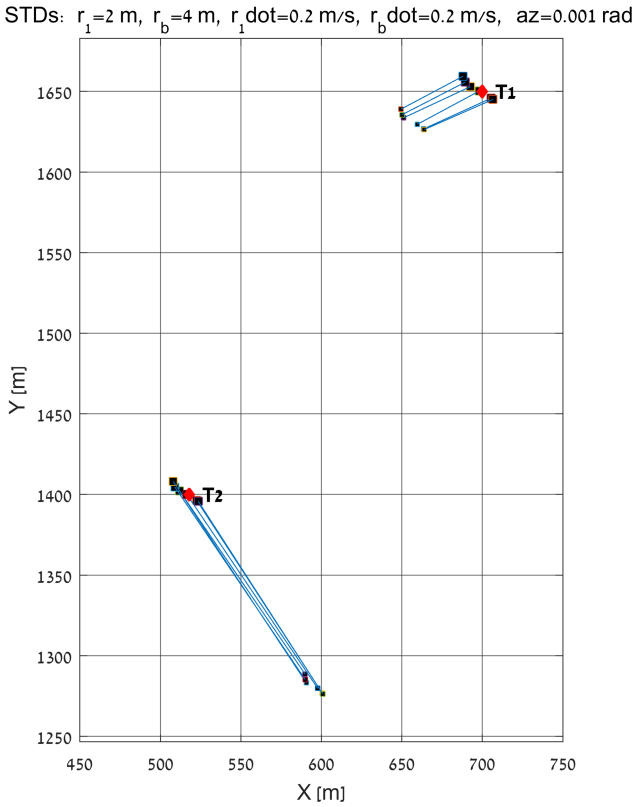

Fig. 12 *Estimated positions and velocities of two targets, obtained in seven simulation runs. Same parameters but different random seeds. The true positions appear as red diamonds*

The proposed scheme is perhaps the simplest 2D case of a DRS using a DRN.

Being a simple system it allowed a detailed demonstration of calculating the target's position and velocity vector from the combined set of measurements, taken simultaneously at two locations. The paper also provided a GDOP contour map of the resulted target's velocity errors. Also discussed was the issue of possible erroneous fusing of data coming from two sources, when two (or more) targets are illuminated by the radar antenna beam. Two approaches of identifying erroneous association were suggested and demonstrated by simulation.

The approach suggested here may find use in short-range radar scene that changes quickly, of which automotive radar is an example.

7 References

[1] Wurman, J., Heckman, S., Boccippio, D.: 'A bistatic multiple-Doppler radar network', *J. Appl. Meteorol.*, 1993, **32**, pp. 1802–1814

[2] Wurman, J., Randal, M., Frush, C.L, *et al.*: 'Design of a bistatic dual-Doppler radar for retrieving vector winds using one transmitter and a remote low-gain passive receiver', *Proc. IEEE*, 1994, **82**, (12), pp. 1861–1872

[3] Satoh, S., Wurman, J.: 'Accuracy of wind fields observed by a bistatic Doppler radar network', *J. Atmos. Ocean. Tech.*, 2003, **20**, pp. 1077–1091

[4] Willis, N.J.: '*Bistatic radar*' (SciTech, Raleigh, NC, USA, 2005, 2nd edn.)

[5] Griffiths, H.D., Baker, C.J., Sammartino, P.F., *et al.*: 'MIMO as a distributed radar system', in Li, J., Stoica, P. (Eds): '*MIMO radar signal processing*' (Wiley, Hoboken, NJ, USA, 2009), pp. 319–363

[6] Griffiths, H., 'Passive bistatic radar', in Sidiropoulos, N.D., Gini, F., Chellappa, R. (Eds.): '*Academic press library in signal processing*' (Elsevier, Oxford, UK, 2014), vol. 2, ch. 16, pp. 813–855

[7] Du, Y., Ping, W.: 'An explicit solution for target localization in noncoherent distributed MIMO radar system', *IEEE Signal Process. Lett.*, 2014, **21**, (9), pp. 1093–1097

[8] Wanchun, L., Qiu, T., Chengfeng, H., *et al.*: 'Location algorithm for moving target in non-coherent distributed multiple-input multiple-output radar systems', *IET Signal Process.*, 2017, **11**, (5), pp. 503–514

[9] Ngo, M.T., Gregers-Hansen, V., Ward, H.R.: 'Transmitter noise compensation – a signal processing technique for improving clutter suppression'. IEEE Conf. on Radar, Verona, NY, USA, April 2006

[10] Ai-Ashwal, W.A., Balleri, A, Griffiths, H.D., *et al.*: 'Measurements of bistatic radar sea clutter'. IEEE Radar Conf., Kansas City, MO, USA, May 2011, pp. 217–221

[11] Sorenson, H.W.: '*Parameter estimation – principles and problems*' (Marcel Dekker, New York, NY, USA, 1980)

[12] Lee, H.B.: 'A novel procedure for assessing the accuracy of hyperbolic multilateration systems', *IEEE Trans. Aerosp. Electron. Syst.*, 1975, **11**, (1), pp. 2–15

[13] Torriery, D.J.: 'Statistical theory of passive location systems', *IEEE Trans. Aerosp. Electron. Syst.*, 1984, **20**, (2), pp. 183–198

[14] Levanon, N.: 'Lowest GDOP in 2-D scenarios', *IEE Proc., Radar Sonar Navig.*, 2000, **147**, (3), pp. 149–155

[15] Cohen, I., Elster, R., Levanon, N.: 'Good practical continuous waveform for active bistatic radar', *IET Radar Sonar Navig.*, 2016, **10**, (4), pp. 798–806

[16] Sandberg, J.S., Inggs, M.R.: 'Synchronizing network radar using all-in-view GPS-disciplined oscillators'. IEEE Radar Conf., Seattle, WA, USA, May 2017, pp. 1640–1645

[17] Wang, W.Q.: 'Time and phase synchronization via direct-path signal for bistatic synthetic aperture radar system', *IET Radar Sonar Navig.*, 2008, **2**, (1), pp. 1–11

8 Appendix

8.1 Derivative matrix H

$$\boldsymbol{H} = \begin{bmatrix} \frac{\partial r_1}{\partial x} & \frac{\partial r_1}{\partial y} & \frac{\partial r_1}{\partial v_x} & \frac{\partial r_1}{\partial v_y} \\ \frac{\partial r_b}{\partial x} & \frac{\partial r_b}{\partial y} & \frac{\partial r_b}{\partial v_x} & \frac{\partial r_b}{\partial v_y} \\ \frac{\partial \dot{r}_1}{\partial x} & \frac{\partial \dot{r}_1}{\partial y} & \frac{\partial \dot{r}_1}{\partial v_x} & \frac{\partial \dot{r}_1}{\partial v_y} \\ \frac{\partial \dot{r}_b}{\partial x} & \frac{\partial \dot{r}_b}{\partial y} & \frac{\partial \dot{r}_b}{\partial v_x} & \frac{\partial \dot{r}_b}{\partial v_y} \\ \frac{\partial \alpha}{\partial x} & \frac{\partial \alpha}{\partial y} & \frac{\partial \alpha}{\partial v_x} & \frac{\partial \alpha}{\partial v_y} \end{bmatrix} \tag{16}$$

$$\frac{\partial r_1}{\partial x} = \frac{x - x_1}{r_1} \tag{17}$$

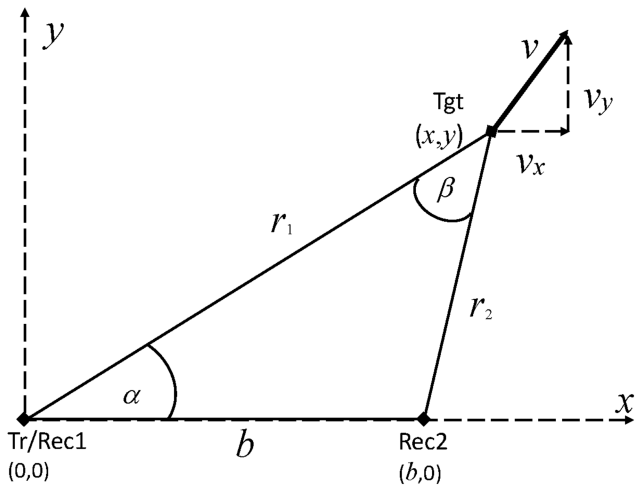

Fig. 13 *Definitions for the direct solution*

$$\frac{\partial r_1}{\partial y} = \frac{y - y_1}{r_1} \tag{18}$$

$$\frac{\partial r_1}{\partial v_x} = 0, \quad \frac{\partial r_1}{\partial v_y} = 0 \tag{19}$$

$$\frac{\partial r_b}{\partial x} = \frac{x - x_1}{r_1} + \frac{x - x_2}{r_2} \tag{20}$$

$$\frac{\partial r_b}{\partial y} = \frac{y - y_1}{r_1} + \frac{y - y_2}{r_2} \tag{21}$$

$$\frac{\partial r_b}{\partial v_x} = 0, \quad \frac{\partial r_b}{\partial v_y} = 0 \tag{22}$$

$$\dot{r}_i = \frac{\mathrm{d}r_i}{\mathrm{d}t} = \frac{v_x(x - x_i) + v_y(y - y_i)}{r_i} \tag{23}$$

$$\frac{\partial \dot{r}_i}{\partial x} = \frac{v_x}{r_i} - \frac{\dot{r}_i(x - x_i)}{r_i^2}, \quad i = 1, 2 \tag{24}$$

$$\frac{\partial \dot{r}_i}{\partial y} = \frac{v_y}{r_i} - \frac{\dot{r}_i(y - y_i)}{r_i^2} \quad , i = 1, 2 \tag{25}$$

$$\frac{\partial \dot{r}_i}{\partial v_x} = \frac{x - x_i}{r_i}, \quad i = 1, 2 \tag{26}$$

$$\frac{\partial \dot{r}_i}{\partial v_y} = \frac{y - y_i}{r_i}, \quad i = 1, 2 \tag{27}$$

$$\frac{\partial \dot{r}_b}{\partial x} = \frac{\partial \dot{r}_1}{\partial x} + \frac{\partial \dot{r}_2}{\partial x} \tag{28}$$

$$\frac{\partial \dot{r}_b}{\partial y} = \frac{\partial \dot{r}_1}{\partial y} + \frac{\partial \dot{r}_2}{\partial y} \tag{29}$$

$$\frac{\partial \dot{r}_b}{\partial v_x} = \frac{\partial \dot{r}_1}{\partial v_x} + \frac{\partial \dot{r}_2}{\partial v_x} \tag{30}$$

$$\frac{\partial \dot{r}_b}{\partial v_y} = \frac{\partial \dot{r}_1}{\partial v_y} + \frac{\partial \dot{r}_2}{\partial v_y} \tag{31}$$

$$\frac{\partial \alpha}{\partial x} = \frac{-(y - y_1)}{r_1^2} \tag{32}$$

$$\frac{\partial \alpha}{\partial y} = \frac{x - x_1}{r_1^2} \tag{33}$$

$$\frac{\partial \alpha}{\partial v_x} = 0, \quad \frac{\partial \alpha}{\partial v_y} = 0 \tag{34}$$

8.2 Direct solution using four measurements $[r_1, \dot{r}_1, \dot{r}_b, \alpha]$

Given the measurements $[r_1, \dot{r}_1, \dot{r}_b, \alpha]$, a direct solution for the target location $[x, y]$ and velocity vector $[v_x, v_y]$ can be derived, by defining these parameters (Fig. 13)

$$r_2 = \sqrt{r_1^2 + b^2 - 2r_1 b \cos\alpha} \tag{35}$$

$$\dot{r}_2 = \dot{r}_b - \dot{r}_1 \tag{36}$$

The target location can easily be calculated as

$$\begin{cases} x = r_1 \cos\alpha \\ y = r_1 \sin\alpha \end{cases} \tag{37}$$

Using the relation for the range rates

$$\begin{cases} \dot{r}_1 = \dfrac{v_x x + v_y y}{r_1} \\ \dot{r}_2 = \dfrac{v_x(x - b) + v_y y}{r_2} \end{cases}, \tag{38}$$

the velocity vector is calculated as

$$\begin{cases} v_x = \dfrac{r_1 \dot{r}_1 - r_2 \dot{r}_2}{b} \\ v_y = \dfrac{-r_1(x - b)\dot{r}_1 + r_2 x \dot{r}_2}{yb} \end{cases} \tag{39}$$